**Proceedings 10th NUMGE 2023**
10th European Conference on Numerical Methods in Geotechnical Engineering
Zdravkovic L, Kontoe S, Taborda DMG, Tsiampousi A (eds)


https://doi.org/10.53243/NUMGE2023-37

# A time-to-fracture DEM model for simulating creep in rough crushable sand

Jiangtao Lei[1], Marcos Arroyo[1], Matteo Ciantia[2], Ningning Zhang[3]

[1]*Department of Geotechnical Engineering and Geosciences, Polytechnic University of Catalonia (UPC), Barcelona, Spain*

[2] *School of Science and Engineering, University of Dundee, Dundee, UK*

[3] *Institute of Geomechanics and Underground Technology, RWTH Aachen University, Aachen, Germany*

**ABSTRACT:** A contact model able to capture creep of crushable sands within a discrete element method (DEM) framework is presented. Time dependency is established through stress-corrosion induced grain fracture. This is grafted onto a pre-existing particle-splitting model developed to simulate rough-crushable sands. The model is calibrated for Fontainebleau sand and applied to simulate soil creep at high-confining pressures. Creep simulation is advanced using the off-DEM ageing technique. The crack-velocity evolution in particle scale and laboratory oedometer creep curve were successfully captured. Moreover, the onset of creep failure during triaxial creep curve under high deviatoric stress can also be simulated using this model. The results obtained indicate significant potential of this model for micromechanically based investigation of time-dependent soil behaviour.

**Keywords:** DEM simulation; Sand creep; Particle breakage; Crack propagation; Off-DEM ageing.

## 1 INTRODUCTION

Sand creep has been well recognized as the causing mechanism for many phenomena of engineering significance, e.g., capacity increase of driven piles in sands (e.g. Gavin and Igoe, 2021). Physical modifications on grains such as grain breakage at high-stress levels are at the root of sand creep (Karimpour & Lade, 2010).

Because of its intrinsic ability to simulate macroscale phenomena based on microscales information, the discrete element method (DEM) seems a promising tool to explore the characteristics of granular creep. Nevertheles, to fulfil that promise, it is necessary to overcome some serious obstacles relating to model calibration and numerical solution procedures.

Kuhn and Mitchell (1993), proposed a visco-frictional contact model, in which the tangential force acting at contacts relaxed in time with a rate that was dependent on mobilized contact friction at the same contact. The model was justified using rate process theory (RPT), by reference to atomic-scale interactions at solid contacts (silica-silica bonds), activated through thermal energy. This model has been often used to simulate creep in DEM (Kwok and Bolton, 2010). Apart from that, the contact creep models, which include the burgers model the maxwell model, or a combination of these two (e.g. Wang et al., 2014) were also adopted to simulate creep in DEM. However, these models are hard to transfer into engineering practice as the micromechanical model parameters lack a clear connection with accessible measurands and can be onlycalibrated by matching the results of specimen-scale experiments, in a complicated and slow process.

An interesting alternative is offered by models explaining creep through delayed particle breakage (e.g. Kwok and Bolton, 2013). Tapias et al., (2015) proposed a crack propagation model based on Charles (1958) law:

$$v = v_0(\frac{K}{K_c})^n \quad (1)$$

where $v$ is crack velocity, $v_0 \approx 0.1$ *m/s* is the reference velocity, $K_c$ is the toughness, $K$ is the stress intensity factor, and $n$ is the stress corrosion index or parameter. However, these works had some problems that made them unpractical for large-scale modelling. To begin with, they both modelled grains using breakable agglomerates. Independently of other questions this is very demanding from a computational viewpoint, particularly if grain size evolution is to be tracked. Besides, Kwok and Bolton (2013) applied fracture to the agglomerate bonds, which made the connection with specimen scale facture parameters more difficult to identify.

A separate problem of creep modelling using DEM is that relatively long creep periods cannot be directly addressed using a numerically stable explicit time step. Precedent work (Kwok & Bolton, 2013; Tapias et al. 2015) got around this problem by directly scaling time mapping timestep into simulated time. This approach curtails the necessary flexibility in computational timestep that is required when addressing evolving grain size distributions at varied confining pressures.

In this work we describe how a stress corrosion model was incorporated into an existing rough-crushable model, based on the particle-splitting technique to simulate soil creep. We also describe how an off-DEM aging technique was implemented to accelerate computation of long creep periods.

## 2 MODEL DESCRIPTION

A three-staged equation (details in Otsubo et al., 2017) to describe the influence of particle roughness on contact stiffness was incorporated into the crushable model described by Ciantia et al. (2019), and has been calibrated by Zhang et al. (2021) to capture the mechanical behaviour and particle size distribution (PSD) evolution of laboratory Fontainebleau NE34 sand, a kind of quartz sand. Particle failure description which is based on the Hertzian contact model is shown in Equation. (2), and the right hand of Equation. (2) is $F_{\text{lim}}$:

$$F_n \leq \sigma_{lim,0} \left(\frac{d}{d_0}\right)^{\frac{-3}{m}} f(var)\pi r'\delta \quad (2)$$

where $F_n$ is the contact normal force, $\sigma_{lim,0}$ is particle strength at reference diameter $d_0$, $f(var)$ is the particle strength variability ; $f(var)$ =$X$*$var$+1, where $X$ is a normalised Gaussian distribution of particle strength and $var$ is the coefficient of variation; $d$ is the sphere diameter, $m$ is the material parameter, and $r' = (\frac{1}{r_1}+\frac{1}{r_2})^{-1}$; $r_1$ and $r_2$ are radius of two contact particles. $\delta$ is contact overlap.

This instantaneous breakage process is complemented by a time-dependent one based on stress corrosion. To this end particles are endowed with initial cracks that grow during simulation following an adapted version of Charles (1958) law:

$$v = v_0(\frac{\sigma}{\sigma_{lim}})^n \quad (3)$$

where σ is the maximum normal contact stress acting on a ball, and particle strength $\sigma_{lim}$=$\sigma_{lim,0} \left(\frac{d}{d_0}\right)^{\frac{-3}{m}} f(var)$, $v$, $v_0$, and $n$ are the same as those defined in Equation (1).

Crack half-length $a$ can be updated every time-interval $\Delta_t$ as:

$$a = a_0 + v \times \Delta_t \quad (4)$$

where $a_0$ is initial crack-half length of a particle, and follows a random uniform distribution ranging from 0.001$d$ to 0.5$d$, where $d$ is particle diameter.

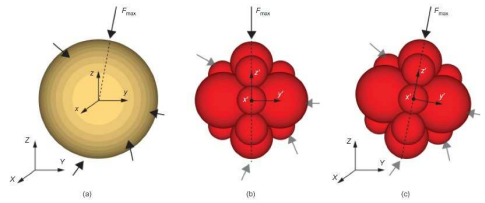

*Figure 1. Particle splitting scheme (Ciantia et al., 2015) (a. the particle with five contact force; b. 14 siblings; c. silbling rotation)*

Once $F_n$> $F_{\text{lim}}$ or $a$>0.5$D$, the particle will split into 14 balls, and follows the sibling rotation to the direction of normal component of maximum contact force as shown in Figure 1. To ensure computational efficiency, a particle comminution limit (diameter), $d_c$=0.1155 mm, is imposed to stop the crushing of smaller particles.

## 3 PARAMETER SELECTION

Fontainebleau sand representative volumetric element (REV) with the length of 4mm was generated using radius expansion method as shown in Figure 2.

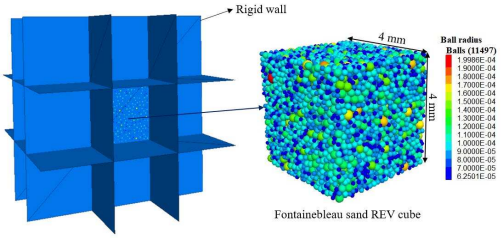


*Figure 2. Fontainebleau sand REV cube*

The REV contains 11497 particles, and particle sizes were designed to match closely to the laboratory PSD for Fontainebleau NE34 sand (Luong and Tuati 1983). The initial void ratio is 0.65 which is equal to 65% relative density of Fontainebleau NE34 sand. Boundaries of the REV cube were set as rigid walls as shown in Figure 2.

*Table 1 Model parameters for Fontainebleau sand REV*

| Category | Parameter/unit | Value |
|---|---|---|
| Particle failure criteria | $G$/GPa | 32 |
| | ν | 0.19 |
| | μ | 0.275 |
| | $m$ | 12 |
| | $\sigma_{lim,0}$/GPa | 3.75 |
| | $var$ | 0.38 |
| | $d_c/d_{50}$ | 0.55 |
| | $d_{max}$/mm | 0.27 |
| | $d_{min}$/mm | 0.01 |
| Contact roughness | $S_q$/μm | 0.6 |
| | $n_1$ | 0.05 |
| | $n_2$ | 5 |
| Crack Propagation | $v_0$ | 0.1 |
| | $n$ | 60 |

Note: $G$=shear modulus; ν= Poisson's ratios; μ= interparticle friction coefficient; $dc$= particle comminution limit; $d_{50}$=50% pass particle size; $d_{max}$, $d_{min}$=maximum, minimum particle diameter; $S_q$=particle surface roughness; $n_1$, $n_2$= roughness parameters

The model parameters regarding immediate particle breakage and roughness were calibrated by Zhang et al. (2021), and are shown in Table 1. A significant advantage of incorporating roughness to the contact model is that the value of the shear modulus $G$ adopted is very similar to that of the real quartz, and it does not need to be calibrated by matching macroscopic stiffness.

For rocks in general, the stress corrosion index is highly sensitive to a number of ambient factors, such as stress level, temperature, presence and chemistry of a pore fluid (Brantut et al. 2013). The sensitivity of stress corrosion to water content is also highly dependent on compositional factors. Limestones are highly sensitive to water presence (Olson et al. 2002). In sandstones the presence of a small clay fraction enhances very much the effect of water (Nara et al. 2012) and, as quartz dominates the composition, the effect of water is less significant (Olson et al. 2002). A stress corrosion index value n = 60 was selected as a pragmatic choice for this study of quartz sands.

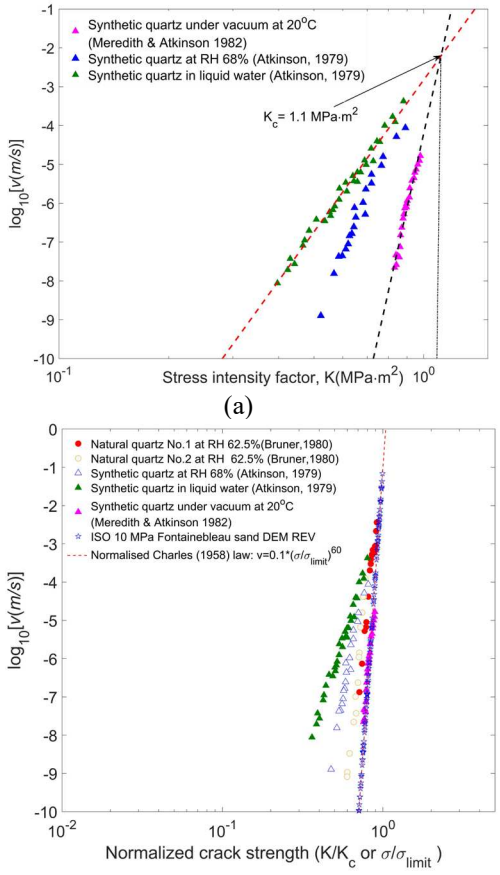


*Figure 3. Model verification in particle scale (a)analysis of K-v (crack velocity) relationship for laboratory synthetic quartz (b) normalized K-v behaviour comparison*

Figure 3(a) shows the $K$-$v$ relationship analysis of laboratory synthetic quartz sand. The linear regression for two extreme cases (RH=0% and RH=100%) was carried out, and $K_c$ should be the intersection of two lines according to Equation (1), which is 1.1 MPa·m$^{0.5}$. Moreover, Tapias (2016) adapted the data for natural quartz and find $K_c$ for natural quartz is also 1.1 MPa·m$^{0.5}$. By knowing $K_c$ of real quartz sand and $\sigma_{lim}$ of DEM particles, the normalized particle crack strength of experimental results and DEM simulations can be compared. This is achieved by isotropically loading the REV cube to 10 MPa to ensure it is at particle breakage dominant state; then, particles in the REV cube whose crack velocity falls into the scale of experimental results can be selected and compared as shown in Figure 3(b). It can be seen from Figure 3(b) that the $K$-$v$ behaviour of particles in DEM simulation is highly consistent with those of synthetic quartz under vacuum (RH=0%) and at room temperature (20°C). It means that Charles law is correctly implemented in the DEM model.

## 4 OFF-DEM AGEING

Dynamic DEM computation advances explicitly in time. Computational stability requirements limit the time step to values that in most circumstances are well below 10$^{-6}$ s (Otsubo et al. 2017b). Due to the small time-step required by DEM, it is thus impossible to simulate creep by conducting only a dynamic computation. Therefore, Off-DEM ageing technique is proposed in this study to accelerate simulation as shown in Figure 4. This on-off computational strategy had been previously applied in some DEM (Tran et al. 2009) or FEM-DEM models (Ma et al. 2015) of rockfill fracture-induced time evolution. It has also strong analogies with the high-cycle continuum models (Niemunis et al. 2005) applied to evaluate the effect of long-term cyclic loads.

The flowchart illustrated in Figure 4 shows that creep simulation starts from dynamic computation in PFC software, and the minimum cycling number was determined as 150,000 to ensure the equilibrium of the sample (vertical stress stops fluctuation). After that, the time $\Delta t_{DC}$, the crack velocity $v_{DC\_end}$ and the crack half-length $a_{DC\_end}$ at the end of dynamic computation are recorded, and it turns to off-DEM ageing.

Crack propagation is assumed at a constant velocity during off-DEM ageing, and the velocity should be $v_{DC\_end}$ of previous dynamic computation. Therefore, crack propagation procedure can be carried out outside PFC. The essence of this Off-DEM ageing is to add a crack increment $\Delta a$ directly to all particles, and this crack increment depends on $v_{DC\_end}$ of each particle and ageing time $\Delta t_{\mathrm{OffD}}$:

$$\Delta a = v_{DC\_end} \times \Delta t_{OffD} \quad (6)$$

Off-DEM ageing would eventually lead to particle breakage. The number of broken particles is controlled

during each Off-DEM ageing period to limit dynamical disruption, as analysed in Section 5. To achieve this, if continue assumed that crack velocity would keep constant until particles are broken, each particle would have its particle failure time $\Delta t$:

$$\Delta t = \frac{r - a_{DC\_end}}{v_{DC\_end}} \tag{7}$$

where $r$ is particle radius, $v_{DC\_end}$ and $a_{DC\_end}$ is crack velocity and crack half-length at the end of the previous dynamic computation.

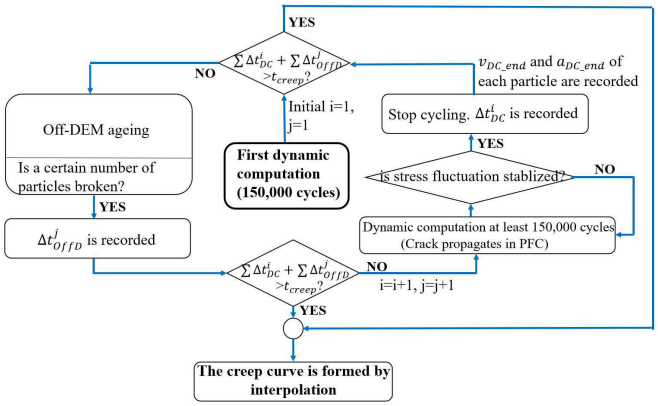


*Figure 4. Flowchart for off-DEM ageing technique*

By listing $\Delta t$ of all particles and reordering them from minimum to maximum as shown in Figure 5, it can be seen that if selecting $t_{\mathrm{OffD}}$ as $\Delta t1$, there will be 3 particles to break.

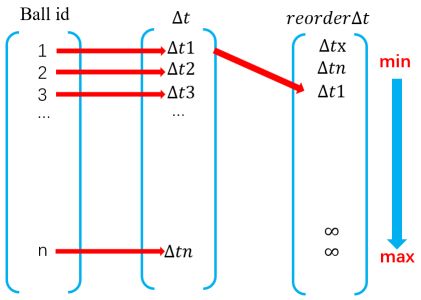


*Figure 5. Controlling the number of broken particles during the time-skipping stage*

After finishing Off-DEM ageing, the ageing time $\Delta t_{offD}$ is recorded. As shown in Figure 5, once $\sum \Delta t_{DC} + \sum \Delta t_{offD}$ is equal to target creep time $t_{creep}$, the Off-DEM ageing workflow is finished, and the creep curve can be formed using interpolation.

## 5 CREEP SIMULATION

### 5.1 Oedometer creep

Results of an oedometer creep stage simulation are presented to illustrate the performance of the Off-DEM ageing scheme described in Section 4. To compare DEM results with the existing laboratory results of vacuum quartz sand ($d$=378±22$\mu m$; Brzesowsky et al., 2014), the design creep vertical stress was 21.7 MPa.

Figure 6 shows the simulation results of oedometer creep. Red points mark results of dynamic computation and the period between two points corresponds to Off-DEM ageing period. It can be seen in Figure 6 that the creep trend of laboratory vacuum-dried quartz sand is very similar to the DEM results.

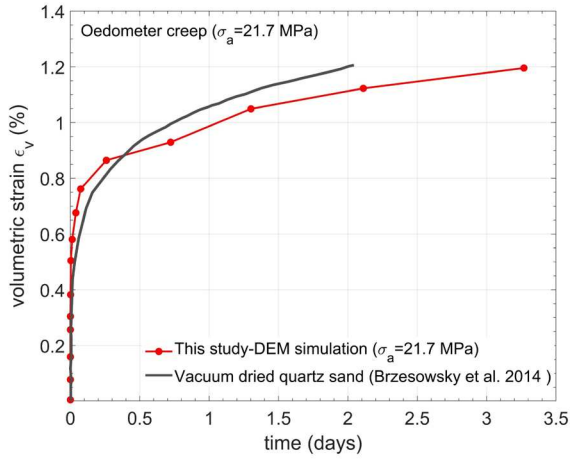


*Figure 6. Oedometer creep simulation*

### 5.2 Dynamic fluctuation

During dynamic computation, the target vertical stress is controlled by continually adjusting the top wall position using a stress-controlled scheme. This result in a vertical stress fluctuation that accompanies the generation of creep strains during the DEM computation, as shown in Figure 7.

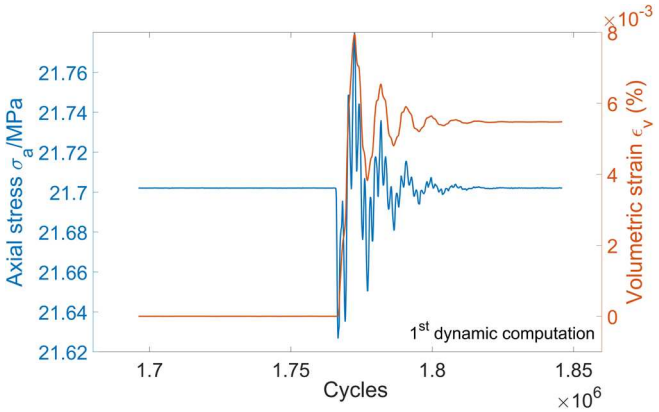


*Figure 7. Axial stress and volumetric strain changing during 1st dynamic computation (30 broken particles)*

The amplitude of these dynamic fluctuation upon resstarting computation should remain moderate, to maintain the creep stress within reasonable bounds. To further analyse this aspect, taking the second dynamic computation as an example, the number of broken particles of the previous Off-DEM ageing stage was controlled to check its influence on vertical stress fluctuation as shown in Figure 8.

It can be seen from Figure 8(a) that the fluctuation amplitude of vertical stress growths rapidly with the number of particles broken upon restarting, and the fluctuation pattern is similar apart from the amplitude. Therefore, controlling the number of accumulated broken particles during off-DEM aging periods the stress fluctuation amplitude during the dynamic computation phases may be controlled. To further analyse this, the average absolute value of maximum fluctuation amplitude $\sigma_{max}$ and minimum fluctuation amplitude $\sigma_{min}$ under different numbers of broken particles is plotted in Figure 8(b). It can be seen that when the number of broken particles is less than 30, the influence of broken particles on vertical stress fluctuation becomes less obvious, and the average fluctuation amplitude is also smaller than 0.5 MPa. Therefore, considering this and the simulation efficiency, the number of broken particles allowed during each off-DEM aging was limited to 30.

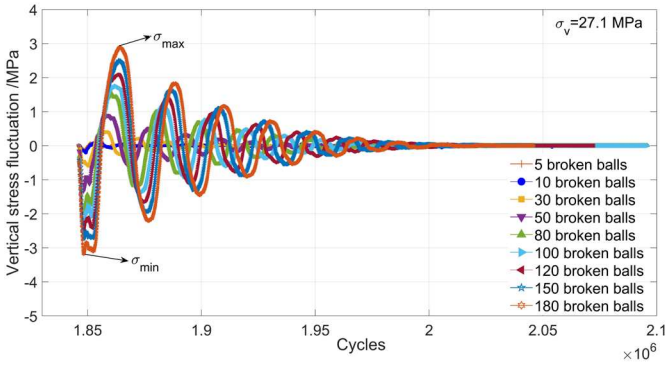


(a)

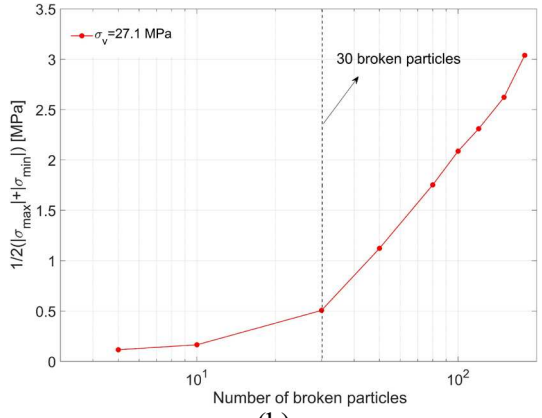


(b)

*Figure 8. Sample disruption analysis (a) vertical stress fluctuation (b) number of broken particles vs vertical stress fluctuation amplitude.*

## 5.3 *Triaxial creep*

To conduct triaxial creep, the REV was first isotropically loaded to 10 MPa to ensure it was at breakage dominant state. Afterwards, a standard triaxial compression test was conducted to identify the maximum deviatoric stress $q_{max}$ (22.6 MPa). Triaxial creep was carried out at different levels of mobilized strength $q/q_{max}$ ($q$ is deviatoric stress), and it is achieved by continually adjusting six walls' positions to maintain constant stress state.

Figure 9 shows representative triaxial creep results. For creep stages at the lower levels of mobilized strength, creep strain remains linear with time in log scale. At the larger level of mobilized strength there is a clear inflection point leading to creep rupture.

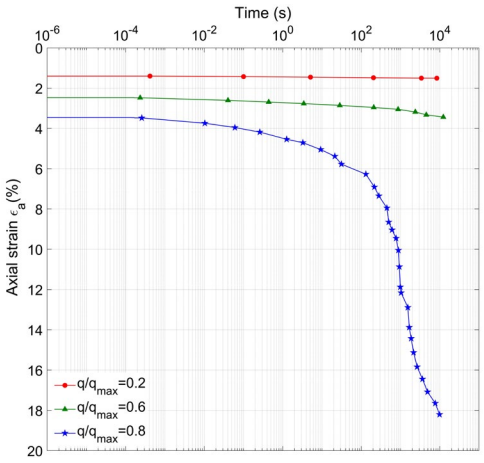


*Figure 9. Triaxial creep of Fontainebleau sand*

A procedure similar to that of oedometer creep was also carried out to verify the influence of the number of broken particles during off-DEM ageing on vertical stress fluctuation. It can be seen from Figure 10 that, for all cases, the average vertical stress fluctuation amplitudes are lower than 0.3 MPa when the number of broken particles is smaller than 30. Therefore, the maximum number of broken particles during each Off-DEM ageing in triaxial creep was also selected as 30.

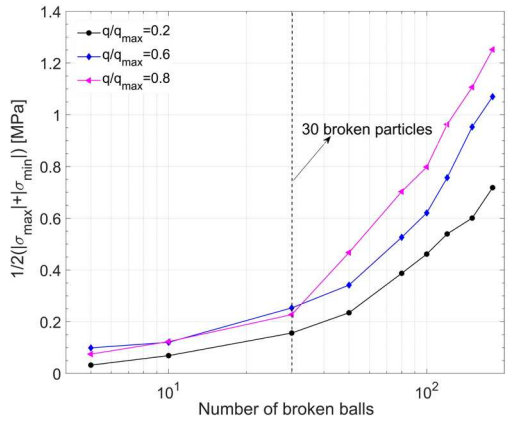


*Figure 10. Influence of broken particles on vertical stress fluctuation in triaxial creep*

Similar to oedometer tests, taking the case of $q/q_{max}$=0.4 and 0.9 as examples, the vertical stress fluctuations of all dynamic computation stages are plotted in Figure 11. It can be seen that when controlling the broken number under 30, the amplitude of the vertical stress fluctuation remains below 2% of the target creep stress.

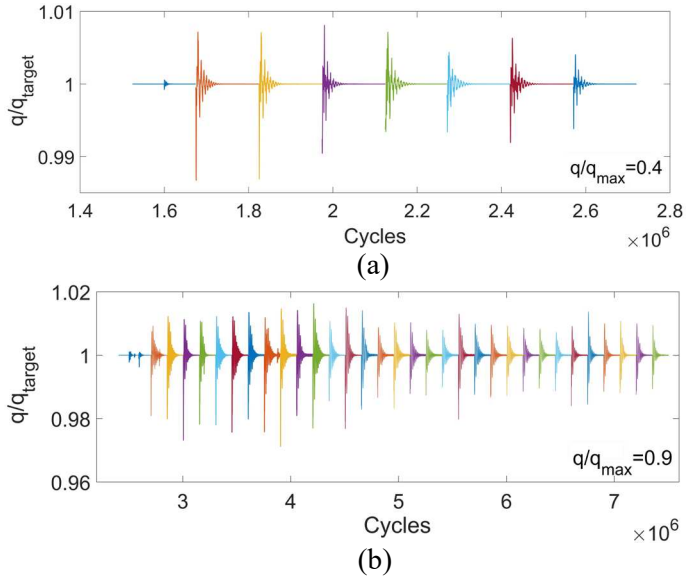


*Figure 11. Vertical stress fluctuations during the dynamic computation stages in triaxial creep phase (a)$q/q_{max}$=0.4 (b) $q/q_{max}$=0.9*

## 6 CONCLUSIONS

This study describes a novel high physically based DEM model developed to simulate time effects in granular soils. The model uses a particle splitting technique and an off-DEM ageing technique to improve computational efficiency. The suitable number of broken particles during off-DEM aging was proved to be under 30. The simulation results compare favourably with the laboratory the oedometer creep result. The traditional triaxial creep behaviour was also be simulated. Further validation and model results are presented by Lei et al (2023).

## 7 ACKNOWLEDGEMENTS

The first author has received support from the Chinese Government Scholarship. (CSC No.202108390006) Spanish Research Agency support (AEI) through research project PID2020-119598RB-I00 is also acknowledged.

## 8 REFERENCES

Atkinson, B.K. 1979. A fracture mechanics study of subcritical tensile cracking of quartz in wet environments, *Pure Appl. Geophys* PAGEOPH **117**, 1011– 1024.

Brantut, N., Heap, M. J., Meredith, P. G., & Baud, P. 2013. Time-dependent cracking and brittle creep in crustal rocks: A review. *Journal of Structural Geology*, *52*, 17-43.

Bruner, W.M. 1980. Effects of time-dependent crack growth on the unroofing and unloading behaviour of rock, PhD. thesis. *University* of California, Los Angeles (USA).

Brzesowsky, R. H., Hangx, S. J. T., Brantut, N., & Spiers, C. J. 2014. Compaction creep of sands due to time-dependent grain failure: Effects of chemical environment, applied stress, and grain size, *J. Geophys. Res.-Sol. Ea.*, **119**(10), 7521–7541. https://doi.org/10.1002/2014JB011277

Charles, R. J. 1958. Static fatigue of glass, *J. Appl. Phys.* ***29***(11), 1549–1560.

Ciantia, M. O., Arroyo, M., Calvetti, F., & Gens, A. 2015. An approach to enhance efficiency of dem modelling of soils with crushable grains, *Géotechnique*, **65**(2), 91–110. https://doi.org/10.1680/geot.13.P.218

Ciantia, M. O., Arroyo, M., O'Sullivan, C., Gens, A., & Liu, T. 2019. Grading evolution and critical state in a discrete numerical model of Fontainebleau sand, *Géotechnique*, ***69***(1), 1–15. https://doi.org/10.1680/jgeot.17.P.023

Gavin, K., & Igoe, D. 2021. A field investigation into the mechanisms of pile ageing in sand, *Géotechnique*, **71**(2), 120–131. https://doi.org/10.1680/jgeot.18.P.235

Kuhn, M. R. & Mitchell, J. K. 1993. New perspectives on soil creep, *ASCE J. Geotech. Engng* **119**(3), 507–524.

Karimpour, H., & Lade, P. v. 2010. Time Effects Relate to Crushing in Sand, *J. Geotech. Geoenviron. Eng.*, **136**(9), 1209–1219.

Kwok, C. Y., & Bolton, M. D. 2010. DEM simulations of thermally activated creep in soils, *Géotechnique*, **60**(6), 425–433. https://doi.org/10.1680/geot.2010.60.6.425

Kwok, C. Y., & Bolton, M. D. 2013. DEM simulations of soil creep due to particle crushing, *Géotechnique,* **63**(16), 1365–1376. https://doi.org/10.1680/geot.11.P.089

Lei, J. , Arroyo, M. , Ciantia, M. & Zhang, N. 2023 A fracture-based discrete model for simulating creep in sand, *submitted*

Meredith, P.G., Atkinson, B.K. 1982. High-temperature tensile crack propagation in quartz: Experimental results and application to time-dependent earthquake rupture, *Earthq. Predict. Res.* **1**, 377–391.

Nara, Y., Morimoto, K., Hiroyoshi, N., Yoneda, T., Kaneko, K., & Benson, P. M. 2012. Influence of relative humidity on fracture toughness of rock: implications for subcritical crack growth. *International Journal of Solids and Structures*, 49(18), 2471-2481.

Olson, J. E., Holder, J., & Rijken, P. 2002, October. Quantifying the fracture mechanics properties of rock for fractured reservoir characterization. In *SPE/ISRM Rock Mechanics Conference*. OnePetro.

Otsubo, M., O'Sullivan, C., Hanley, K. J., & Sim, W. W. 2017. The influence of particle surface roughness on elastic stiffness and dynamic response, *Géotechnique*, **67**(5), 452–459. https://doi.org/10.1680/jgeot.16.P.050

Otsubo, M., O'Sullivan, C., & Shire, T. 2017b. Empirical assessment of the critical time increment in explicit particulate discrete element method simulations. *Computers and Geotechnics*, 86, 67-79.

Tapias, M. 2016. Particle model for crushable aggregates which includes size, time and relative humidity effects, PhD Thesis, *Universitat Politecnica de Catalunya*, Barcelona.https://upcommons.upc.edu/handle/2117/106495

Tapias, M., Alonso, E. E., & Gili, J. 2015. A particle model for rockfill behaviour, *Géotechnique*, **65**(11), 975–994.

Wang, Y. H., Lau, Y. M., & Gao, Y. 2014. Examining the mechanisms of sand creep using DEM simulations, *Granular Matter*, **16**(5), 733–750.

Zhang, N., Ciantia, M. O., Arroyo, M., & Gens, A. 2021. A contact model for rough crushable sand, *Soils Found.*, **61**(3), 798–814. https://doi.org/10.1016/j.sandf.2021.03.002